On the urban geometry generalization for CFD simulation of gas dispersion from chimneys: Comparison with Gaussian plume model

Francisco Toja-Silva [a,b,*], Carla Pregel-Hoderlein [a], Jia Chen [a]

[a] Environmental Sensing and Modeling, Technische Universität München (TUM), Theresienstr. 90, 80333 Munich, Germany
[b] Barcelona Supercomputing Center (BSC), Nexus II Building - Jordi Girona 29, 08034 Barcelona, Spain

ARTICLE INFO

ABSTRACT

This article is a contribution to the geometry generalization for computational fluid dynamics (CFD) simulations of gas dispersion in urban areas. The CO_2 emission from a natural gas-fueled thermal power plant is simulated using different generic urban patterns. The buildings distribution, the built density and the height of the buildings were analyzed. Both buildings distribution and built density did not show significant effect on the gas concentration over the city, whereas the average height of the buildings shows a clear influence on the vertical profile of the gas concentration. The results of the general patterns were compared with a real city (Munich, Germany), obtaining agreement between both generalized and real city geometries. Additionally, the vertical profiles of gas concentration were compared with the Gaussian plume model, and a new equation for computing the vertical dispersion parameter is proposed for urban environments as a function of the averaged buildings height.

1. Introduction

As is well known, air pollution is a major problem with strong impact on environment (Clark et al., 2016), economy (Carleton and Hsiang, 2016) and human health (Lelieveld et al., 2015). The urban environment has a great interest because it is where the major anthropogenic emissions take place (Beirle et al., 2011) and where the highest health impact exists (Jerrett et al., 2005). In order to analyze pollutant emissions and their effect on the urban air quality, it is necessary to use modeling techniques combined with on-site measurements (von Schneidemesser et al., 2017; Kiesewetter et al., 2015; Toja-Silva et al., 2017).

The Weather Research and Forecasting (WRF) model is commonly used for the simulation at the meso-scale coupled with pollutant dispersion and photochemical reaction models, e.g. WRF Greenhouse Gas Model (WRF-GHG) (Beck et al., 2011) and Calidad del Aire Operacional para España (CALIOPE) (Baldasano et al., 2008). These meso-scale models reach a finest resolution of around 1 km in the latest developments for urban environments (Feng et al., 2016; Guevara et al., 2017; McKain et al., 2015; Nehrkorn et al., 2013). In order to thoroughly understand emissions, especially in the urban environment, it is necessary to map them on a finer scale (micro-scale simulations), reflecting the dimensions at which carbon is emitted: by individual buildings, vehicles, parks, factories and power plants. Computational Fluid Dynamics (CFD)

is a very powerful tool extensively used nowadays for dealing with the micro-scale simulation of pollutants dispersion in urban environments (Lateb et al., 2016; Tominaga and Stathopoulos, 2013, 2016; Meroney et al., 2016). Several researchers conducted pollutant dispersion CFD simulations for reproducing wind-tunnel simplified problems (e.g. (Takano and Moonen, 2013; Tominaga and Stathopoulos, 2010; Hang et al., 2012; Tang et al., 2006; Tominaga and Stathopoulos, 2007; Yu and Thé, 2016; Gromke and Blocken, 2015; Zhang et al., 2015; Wingstedt et al., 2017)) or for real urban areas (e.g. (Nozu and Tamura, 2012; Patnaik et al., 2007; Jeanjean et al., 2015; Hanna et al., 2006)). When dealing with real cities, the problem becomes complex because it requires a simulation domain bigger than that usually considered in micro-scale simulations, because the emissions in a far region can affect another area, or even the whole city can be the area of study, and there are limitations in micro-scale simulations regarding the geometry complexity and the associated mesh grid density. Additionally, the spatial resolution required in urban environments is finer than that used in meso-scale simulations, because it is important to adequately characterize and locate emission sources, and due to the strong effect of buildings on the fluid flow, i.e. the turbulence associated with the urban boundary layer can increase the plume dilution by a factor of two compared with an open-country exposure (Saathoff et al., 1998). It is clear that a mesh resolution of 1 km cannot accurately reproduce the urban details and
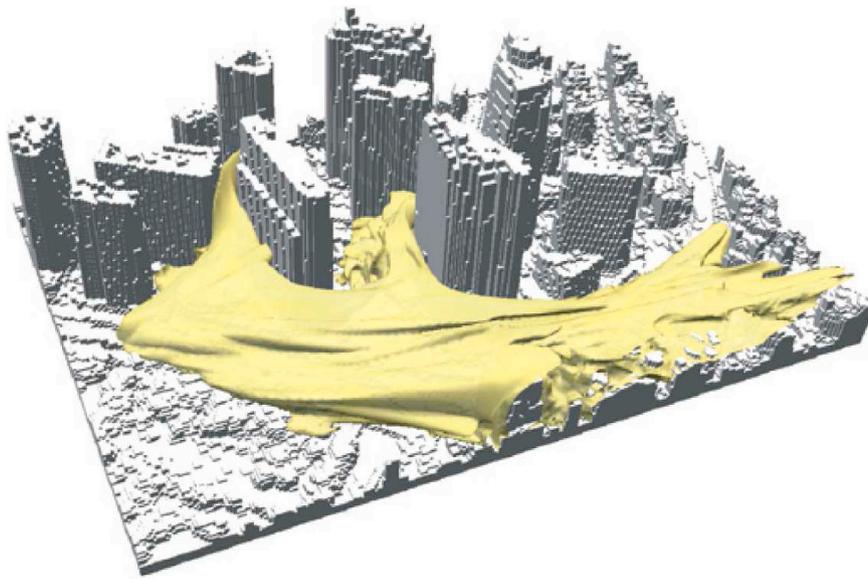

Fig. 1. Realistic domain of the city of Tokyo extracted from GIS, used for CFD simulations. The isosurface corresponds to a polutant release (Nozu and Tamura, 2012).

singularities. Therefore, there is a gap between meso- and micro-scale ranges. With the aim of filling this gap, simplified empirical models are frequently used to deal with this intermediate scale range. Such models are generally based on the Gaussian plume dispersion equations (Bellander et al., 2001), using a more sophisticated formulation in order to deal with multiple sources (both punctual and line sources) and with complex problems as the dispersion phenomena, e.g. AERMOD (Cimorelli et al., 2005), Immission Frequency Distribution Model (IFDM) (Cosemans et al., 1992) and RLINE (Snyder et al., 2013). Although these models are very useful and show reasonably acceptable results for big urban domains, it is important to mention that they are not physical models, i.e. they are not based in physical principles of fluid mechanics and pollutant dispersion but in mathematical formulations derived from physical observations for other cases, under similar conditions when it is possible. Therefore, there is still a necessity of physical models able to deal with this intermediate scale range for several reasons: e.g. for being used to calibrate, develop and improve simplified models, to study particular cases where simplified models show incongruence or differences with observations, and for dealing with complex or potentially high-risk case studies.

The contribution of the present investigation is to bring useful information for using CFD in future simulations dealing with spatial domains and resolutions between micro- and meso-scales, focusing in two types of studies: when the objective is to analyze the gas dispersion around some target buildings immersed in a big urban area, and when the objective is studying the effect of the whole urban area on the gas dispersion, i.e. observed from outside the buildings ensemble. In both cases, it is very useful for making simulations viable to use a general pattern for replacing the detailed geometry (excluding target buildings). Therefore, the objective of this article is to determine which aspects must be considered for the urban geometry generalization in CFD simulations of pollutants dispersion in urban areas. In order to reach this objective, the CO_2 dispersion from a natural gas-fueled thermal power plant is simulated and analyzed using different generic urban patterns. The final results are also compared with an irregular (or non-homogeneous) pattern and with a real city geometry, Munich (Germany). Since we are exploring the upper scale-range limit for CFD, we use Reynolds-Averaged Navier-Stokes (RANS) equations. Large-Eddy Simulation (LES) shows better agreement with wind-tunnel experimental data than RANS, but its computational cost is too high for full-scale big urban areas (Franke et al., 2007). Additionally, due to the high uncertainty present in real urban environments (presence of severe disturbances), the benefits (in terms of

accuracy and others) of using LES instead of RANS for dealing with this application were not scientifically demonstrated yet (Toja-Silva et al., 2017).

Up to the authors' knowledge, this is a completely new approach because CFD was not used before for the analysis of buildings geometry influence on the gas dispersion above the urban canopy with the focus on bigger scales (i.e. the simulation of a whole city). The only precedents are the study of geometry (buildings shape and height) influence on the dispersion between and around (i.e. near surfaces) buildings (Hajra et al., 2011; Chavez et al., 2012; Shen et al., 2017), and inside street canyons from the point of view of street ventilation (Takano and Moonen, 2013; Gu et al., 2657; Nosek et al., 2016; Nosek et al., 2017).

The present investigation extends the research presented in Toja-Silva et al. (2017), where CFD simulations of the CO_2 dispersion over the urban area of Sendling (Munich) were conducted. Such CFD simulations were validated by comparing the results with experimental measurements of column-averaged dry-air mole fraction (Chen et al., 2016, 2017) on the site, and the influence of the turbulent Schmidt number (Sc_t) on the results was studied. Solution verification was also carried out. The case study used for analyzing the real geometry of Munich is extended in the present study to general geometries. In order to be consistent and making fair comparisons, we used the same mesh configuration (i.e. close grid sizes) for simplified and real geometries, yielding a similar computational cost, i.e. no apparent advantage using the simplified geometries. However, the use of a simplified geometry leads to significant advantages when dealing with preprocessing and meshing processes. The real geometry (i.e. Munich) that we are comparing with the general patterns is very clean (e.g. smooth walls), and it required a significant amount of dedication (i.e. high preprocessing cost) for being developed. When the geometry is obtained from other sources, e.g. from Geographical Information Systems (GIS), usually it does not have the same degree of cleanness. As an example, Fig. 1 shows the geometry used by Nozu and Tamura (2012). They used GIS data to simulate the city of Tokyo. They focused on singular high-rise buildings and a more homogeneous surrounding. It is clearly observed that the surrounding buildings have a very complex geometry. Such complexity (especially the irregular surfaces) leads to significant problems for obtaining a high quality mesh. As an alternative to use GIS, considering the results of our investigation, it is possible to represent the singular high-rise buildings with a clean shape and a general simplified pattern for representing the surrounding buildings. Van Hooff and Blocken (van Hooff and Blocken, 2010) also recommends using detailed geometry for target buildings and simplified
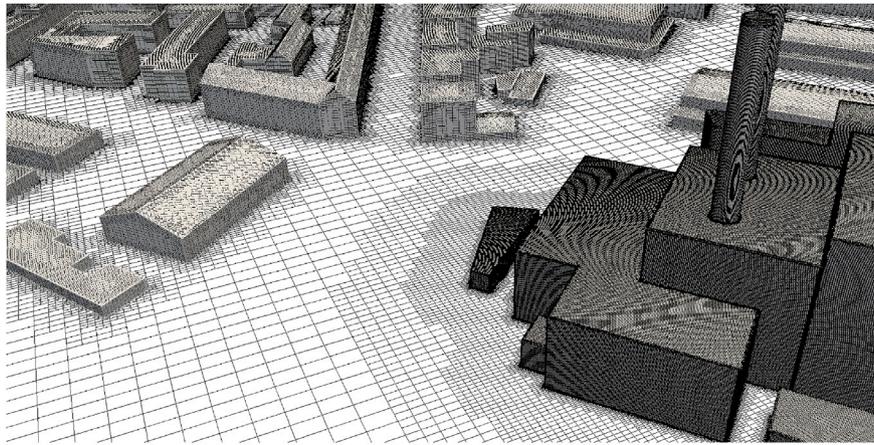
(a) Detail of the mesh, 18.7 M cells

(b) Comparison XCO_2 using 6 different mesh sizes

Fig. 2. Mesh details and grid independence study (Toja-Silva et al., 2017).

geometries for surroundings. Additionally, GIS data could not be available or the geometry can be much more complex when dealing with a bigger area, or with the whole city.

In addition to the geometry generalization study, the vertical profiles of CO_2 concentration obtained in the simulations are used for improving the equation used for computing the vertical dispersion parameter in the Gaussian plume model for urban environments (Briggs, 1973), considering the most relevant characteristics (detected in the present investigation) of the geometry. We compare the results with the Gaussian plume model because, as we commented above, it is frequently used when dealing with the scale range that we are focusing, i.e. between micro- and meso-scales (Seinfeld and Pandis, 2006; Reynolds, 1992).

In what follows, Section 2 discusses about the computational modeling, Section 3 introduces the case study, Section 4 discusses the effect of the buildings distribution, Section 5 analyzes the built density, Section 6 presents an study of the influence of the buildings height on the gas dispersion, and Section 7 shows an example for a heterogeneous pattern. Finally, Section 8 discusses the effect of the urban environment on the dispersion parameters of the Gaussian plume model, and Section 9 presents the conclusions.

2. Computational modeling

The fluid flow (wind) is initially solved using the steady RANS equations (Cheng et al., 2003) (using Einstein notation):

$$\frac{\partial \overline{u}_i}{\partial x_i} = 0, \tag{1}$$

$$\frac{\partial (\overline{u}_i \overline{u}_j)}{\partial x_j} = -\frac{1}{\rho} \frac{\partial \overline{p}}{\partial x_i} + \frac{\partial}{\partial x_j} \left(\nu \frac{\partial \overline{u}_i}{\partial x_j} - \overline{u'_i u'_j} \right), \tag{2}$$

$$\frac{\partial (\overline{u}_j k)}{\partial x_j} = \frac{\partial}{\partial x_j} \left[\left(\nu + \frac{\nu_t}{\sigma_k} \right) \frac{\partial k}{\partial x_j} \right] + P_k - \varepsilon \tag{3}$$

and

$$\frac{\partial (\overline{u}_j \varepsilon)}{\partial x_j} = \frac{\partial}{\partial x_j} \left[\left(\nu + \frac{\nu_t}{\sigma_\varepsilon} \right) \frac{\partial \varepsilon}{\partial x_j} \right] + C_{\varepsilon 1} \frac{\varepsilon}{k} P_k - C_{\varepsilon 2} \frac{\varepsilon^2}{k}, \tag{4}$$

where $\overline{u}$ is the time-averaged velocity, $\overline{p}$ is the mean pressure, ρ the fluid density, ν the kinematic viscosity, ν_t is the kinematic eddy viscosity, k is the turbulence kinetic energy (TKE), $\overline{u'_i u'_j}$ are Reynolds stresses (related to TKE for RANS), $P_k = \nu_t S^2$ is the production of TKE, S is the modulus of the mean rate of strain tensor, and ε is the turbulence dissipation. The coefficients used in the equations are $C_\mu = 0.09$, $C_{\varepsilon 1} = 1.44$, $C_{\varepsilon 2} = 1.92$, $\sigma_k = 1.0$ and $\sigma_\varepsilon = 1.3$.

The Durbin $k - \varepsilon$ turbulence model (Durbin, 1996) is used for the closure. It was developed from the standard $k - \varepsilon$ model in order to improve the accuracy of simulation results (especially TKE) when dealing with bluff bodies, e.g. buildings in urban environments. It consists in applying a realizability constraint that leads to the bounding of the

(a) Location in Munich (Germany). Adapted from Google Maps (Google).
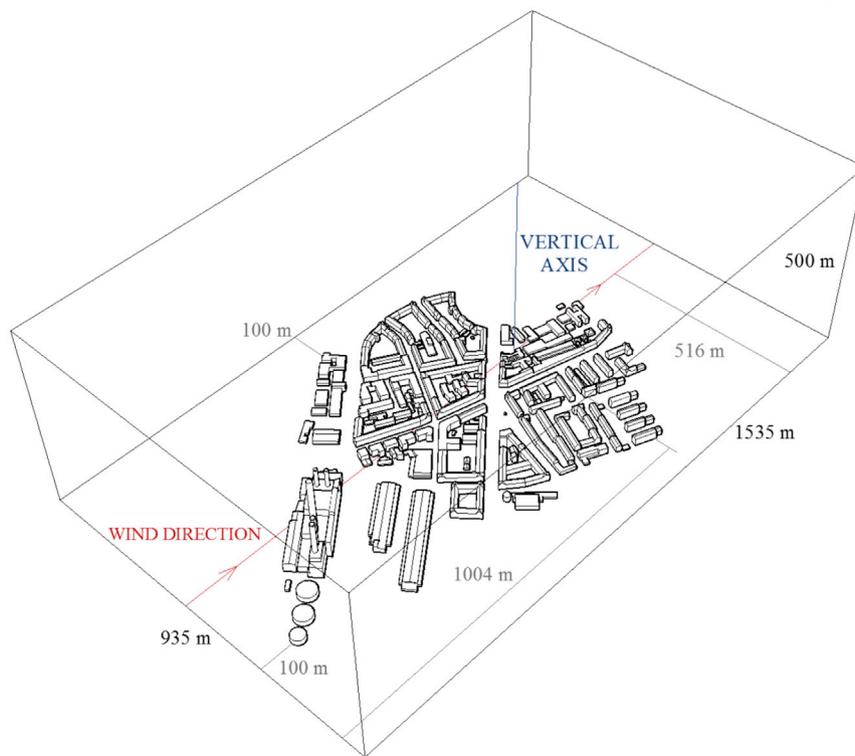
(b) Domain, including the vertical axis (in blue) used for CO_2 concentration comparison. Adapted from Toja-Silva et al. (2017).

**Fig. 3.** Location of the real urban area of study and simulations domain.

turbulence velocity time scale (T) when computing $\nu_t = C_\mu kT$, i.e.

$$T = \min\left(\frac{k}{\varepsilon}, \frac{1}{3C_\mu S}\sqrt{\frac{3}{2}}\right). \qquad (5)$$

The exhaust from the chimneys is considered as air in the fluid flow simulation. We neither consider buoyancy nor use the energy equation because the density difference between exhaust and air is not very significant, and a downwash effect takes place due to the large dimensions of the power plant (i.e. vertical section around 250×50 m) and the

presence of surrounding buildings. We have previously validated this turbulence modeling setting in Toja-Silva et al. (2015) by studying the benchmark case A of the Architectural Institute of Japan (Yoshie et al., 2007; Architectural Institute Japan (AIJ), 2006). This benchmark case consists in an isolated building placed within an atmospheric boundary layer inside of a wind tunnel (experiment of Meng and Hibi (1998)). Hit rates of 87.5% and 75.0% were obtained for wind speed and turbulence kinetic energy (TKE), respectively.
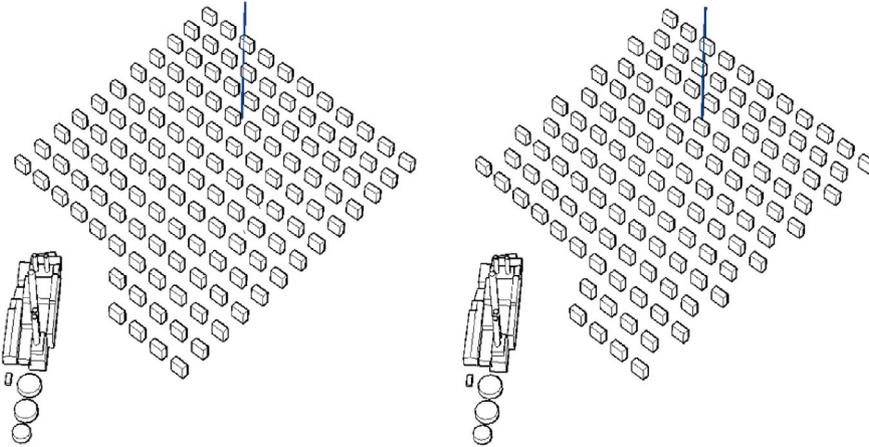
After solving the wind field (i.e. having velocity and turbulence magnitudes), the CO_2 content in the environment (background) is set to
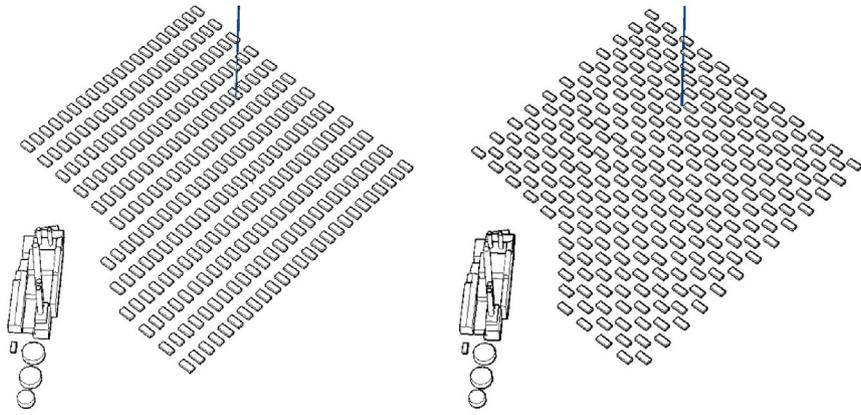
(a) Buildings 5 m height, 17.9 M cells.
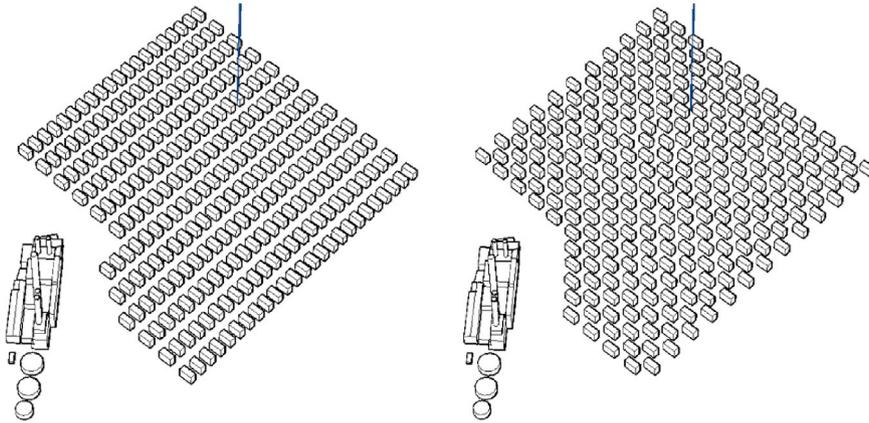
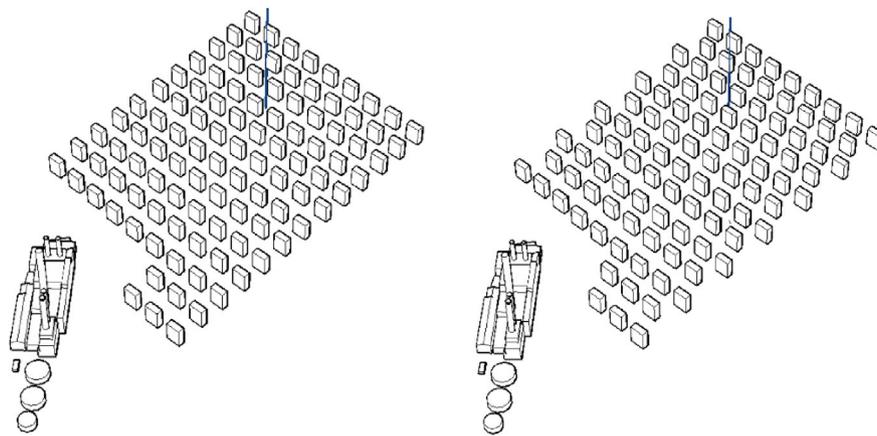(b) Buildings 20 m height, 19.4 M cells.

(c) Buildings 30 m height, 18.3 M cells.

Fig. 4. General view of the general urban patterns compared for the lower buildings: corridor (left) and interpolated (right). The blue line corresponds to the vertical axis used for the CO_2 concentration comparison. The number of mesh cells used for each case is also indicated. (For interpretation of the references to colour in this figure legend, the reader is referred to the web version of this article.)

401.4 ppm. The CO_2 concentration used as boundary condition for chimneys exhaust is 13%. This value could lead to problems for considering CO_2 as trace gas (i.e. passive scalar). However, when the injection takes place, the CO_2 concentration decreases to values below 1% almost immediately due to the large amount of air mass, and it decreases to few thousands of ppm just few tens of meters downstream. Therefore, the gas dispersion problem is solved using the unsteady convection-diffusion passive scalar equation for incompressible turbulent flows (Shen et al., 2002),

$$\frac{\partial C}{\partial t} + \frac{\partial\left(\overline{u_j}C\right)}{\partial x_j} - \frac{\partial}{\partial x_j}\left(\left(D + \frac{\nu_t}{Sc_t}\right)\frac{\partial C}{\partial x_j}\right) = 0, \tag{6}$$

where C is the averaged volumetric CO_2 concentration in parts per million (ppm), $D = 1.6 \cdot 10^{-5}$ m^{2}s^{-1} is the molecular diffusivity (Lide, 2004) and $Sc_t = 0.6$ is the turbulent Schmidt number. We have previously optimized the Sc_t number and validated the gas dispersion modeling in Toja-Silva et al. (2017), by comparing simulation results

(a) Buildings 40 m height, 18.2 M cells.
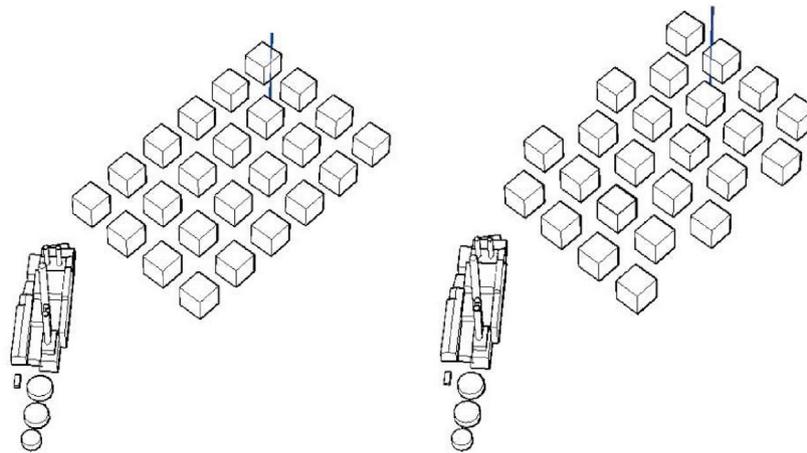
(b) Buildings 50 m height, 17.4 M cells.
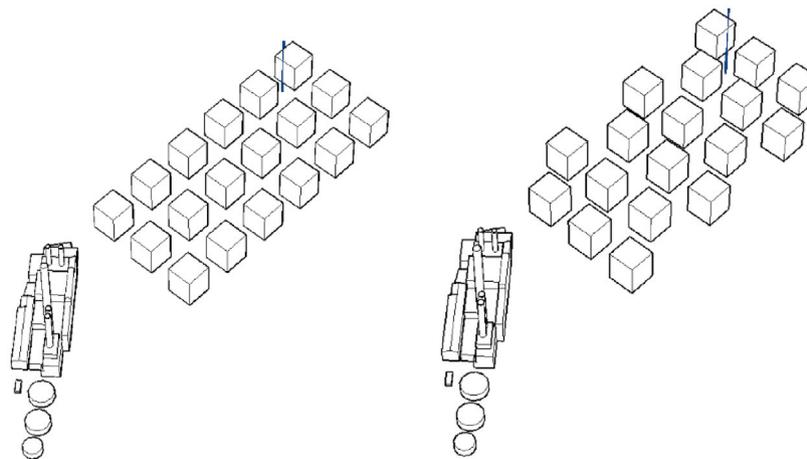
(c) Buildings 60 m height, 17.2 M cells.

Fig. 5. General view of the general urban patterns compared for the higher buildings: corridor (left) and interpolated (right). The blue line corresponds to the vertical axis used for the CO_2 concentration comparison. The number of mesh cells used for each case is also indicated. (For interpretation of the references to colour in this figure legend, the reader is referred to the web version of this article.)
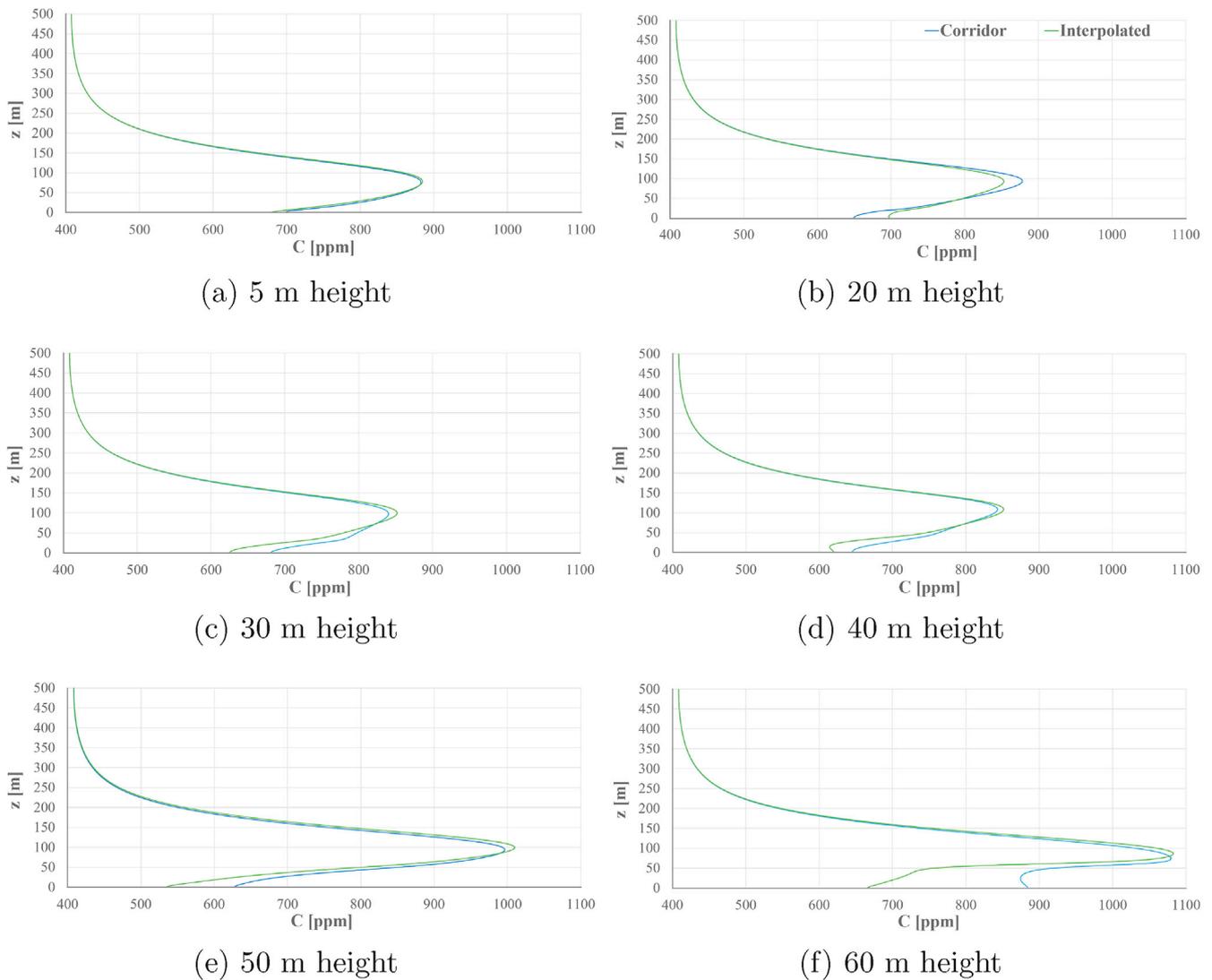
(a) 5 m height

(b) 20 m height

(c) 30 m height

(d) 40 m height

(e) 50 m height

(f) 60 m height

Fig. 6. Vertical profile of CO_2 concentration for corridor vs. interpolated general patterns for different heights.

with experimental measurements of averaged column concentration of CO_2 (XCO_2). As observed in Fig. 2b, the simulation result is inside the error band of the experimental measurement for the configuration used in the simulations (i.e. grid size used).

A self-customized version of the open-source and open-access software OpenFOAM (OpenFOAM) is used for the CFD simulations. The simpleFoam solver for steady-state incompressible turbulent flows is used for solving the fluid flow (RANS equations), and the customized solver turbulentScalarTransportFoam for the gas dispersion (turbulent convection-diffusion passive scalar equation). The simulations are carried out in a Linux cluster using 84 processors.

The inlet wind profiles for velocity (logarithmic), TKE and turbulence dissipation are set according to Richards and Hoxey (1993), with a roughness of $z_0 = 0.2$ m. The von Kármán constant is considered as $\kappa = 0.4$. Since $30 < y^+ < 1000$, standard turbulent wall laws (Blocken et al., 2007; Parente et al., 2011; O'Sullivan et al., 2011) can be used for the treatment of near wall flow. For the ground, sand-grain-based fully rough law of the wall (Blocken et al., 2007) is used, calculating the equivalent sand-grain roughness height according to van Hooff and Blocken (van Hooff and Blocken, 2010) and Toja-Silva et al. (2017). Slip boundary condition is used on the top and both sides, and zero gradient at the outlet. For pressure, zero is imposed at the outlet and zero gradient at the rest of boundaries. The values of velocity and gas concentration from the chimneys are calculated from the emission data. Gas concentration is also

known at the inlet, and zero gradient is imposed at the rest of boundaries.

The spatial discretization of the differential operators is carried out using Gaussian integration with different interpolation schemes. Second order linear interpolation is used for gradients and divergences, and explicit non-orthogonal correction is added for the Laplacian terms. For linear system solvers, generalized geometric-algebraic multi-grid solver (GAMG) with DIC smoother is applied for pressure, and preconditioned bi-conjugate gradient solver for asymmetric matrices (PBiCG) with diagonal incomplete LU (DILU) preconditioner for the rest of variables. The convergence criteria is set to at least 10^{-5} for all the residuals.

The mesh grid is developed in two steps. Initially, we construct a background mesh using the structured blockMesh application of OpenFOAM. In a second stage, the geometry (i.e. power plant and buildings previously designed with a CAD tool and saved in STL format) is embedded into the background mesh using the snappyHexMesh application. The mesh is refined around the buildings and adapted to their shape, with refinement distances of 40 m and 10 m around the power plant and the rest of the buildings, respectively. Fig. 2a shows the mesh used for the real city case. The Richardson extrapolation (Richardson, 1911) for estimating the discretization error cannot be applied in the present case due to the extremely complex geometry, i.e. we have a limitation regarding minimum and maximum number of cells in order to adequately reproduce the geometry (using the grid refinement around buildings) and due to computational resources limitations (we are
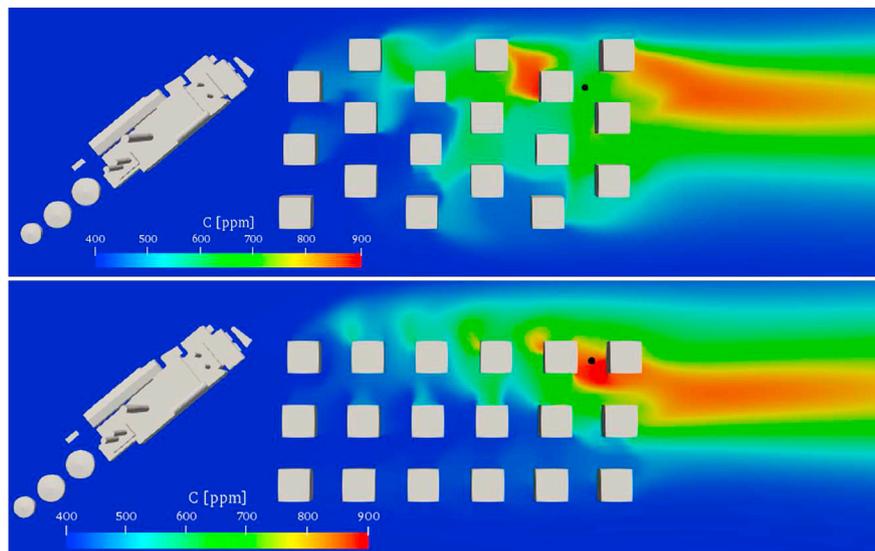
Fig. 7. Horizontal slice of CO_2 concentration around 60 m height buildings at $z = 4$ m for interpolated (top) and corridor (bottom) general patterns. The black point corresponds to the measurement axis in each case.

reaching near 19 M cells), respectively. In order to verify the mesh independence of the solution, we performed a mesh sensitivity analysis, presented in Toja-Silva et al. (2017). Fig. 2b shows an experimental measurement of XCO_2 compared with the simulation results using 6 different mesh sizes: 8.3M, 11.9M, 13.8M, 15.1M, 17.4M and 18.7M cells, respectively. Convergence is clearly observed for $\geq$13.8M cells. Since the configuration corresponding to the finest mesh (18.7M cells) is used in all the computations presented in this article, the mesh independence of the results is guaranteed. Additionally, we have previously verified the order of convergence of the solutions (exhaustive mesh study) using the wind-tunnel model in Toja-Silva et al. (2015), where the hit rate for TKE was analyzed for 3 different meshes (i.e. 1.7 M, 3.1 M and 9.8M cells), yielding a convergence rate of 2.23 and a grid convergence index of 0.0577 (5.77%). Other authors (e.g. Blocken et al. (2004)) also carried out rigorous mesh studies using simplified geometries related to the same problem.

3. The case study

Since the present investigation is an extension of the work of Toja--Silva et al. (2017), the same case study is reproduced varying the buildings geometry. Fig. 3 shows a location map and the geometry of the domain for the real urban case in Sendling (Munich, Germany). The domain sizing was carried out according to the Best Practice Guidelines (Franke et al., 2007).

The goal is to simulate the CO_2 dispersion from a 1.5 GW thermal (natural gas fueled) power plant. The vertical profile of CO_2 concentration at a distance of 500 m is analyzed. The total emission is 43.3 $kgCO_2$ s^{-1}, and the exhaust speed is set to 0.5 m s^{-1} and 2.0 m s^{-1} from North and South chimneys, respectively. The CO_2 content in the exhaust is set to 13% in all cases. The background CO_2 concentration in the environment is set to 401.4 ppm.

The inlet wind profiles (for velocity, turbulence kinetic energy and turbulence dissipation) used are set according to Richards and Hoxey (1993), using the reference wind speed $U_{ref} = 1.38$ m s^{-1} at a reference height $z_{ref} = 30$ m.

4. Effect of buildings pattern on the gas dispersion

In order to analyze the effect of the buildings distribution on the vertical CO_2 profile, two different general patterns are compared, namely

corridor and interpolated as shown at the left and right hand sides of Figs. 4 and 5, respectively. The number of mesh cells used for the simulation of the different geometries is also shown. Corridor and interpolated patterns are compared for different heights, i.e. 5 m, 20 m, 30 m, 40 m, 50 m and 60 m. These two general patterns are frequently used to analyze the effect of urban buildings distribution in other related fields, e.g. urban wind energy (Toja-Silva et al., 2016) and urban microclimate (Shishegar, 2013).

As shown in Fig. 6, above the buildings, small differences in the vertical profile of CO_2 concentration are found between both general patterns (i.e. corridor and interpolated), for buildings of the same height. The largest difference is observed for the case of 20 m height, yielding a maximum difference of 3% for the peak of CO_2 concentration around 90 m height (6.3% with respect to the background concentration). Therefore, we can state that the building distribution is not the determining factor governing the CO_2 dispersion in urban environments.

The most significant difference between the vertical profiles of the general patterns is observed at the ground level, i.e. below the buildings height. Such difference is due to local effects given by the position and the shape of the buildings. As expected, these local effects are more pronounced for higher buildings (Fig. 6f) and they are negligible for short buildings (Fig. 6a). Fig. 7 shows a horizontal slice of the CO_2 around the 60 m height buildings at the ground level (i.e. 4 m height). It is observed that the buildings have an important influence at this level, and the concentration values can vary significantly around the buildings. Therefore, we can state that there is not a significant effect of the buildings configuration on the gas concentration profile above the buildings, but at the ground level (i.e. between the buildings) the buildings position and shape has a strong relevance, especially for high buildings. Thus, it is already clear that the present investigation will be valid only above the urban canopy, and that will be the area of study.

5. Effect of built density on the gas dispersion

In this section, general urban patterns with different densities are compared in order to analyze the effect of the built density on the gas dispersion. The patterns used in this comparison have a height of 20 m. The build density is calculated considering an internal area of around 0.15 km^2 (i.e. 350×420 m) inside the domain, as shown in Fig. 8.

Fig. 9 shows a comparison of the vertical profile obtained for different built densities, with buildings of 20 m height. Again, high differences are

(a) 22.6%, 19.4M cells

(b) 10.4%, 17.9M cells

(c) 8.7%, 17.2M cells

(d) 5.0%, 16.8M cells
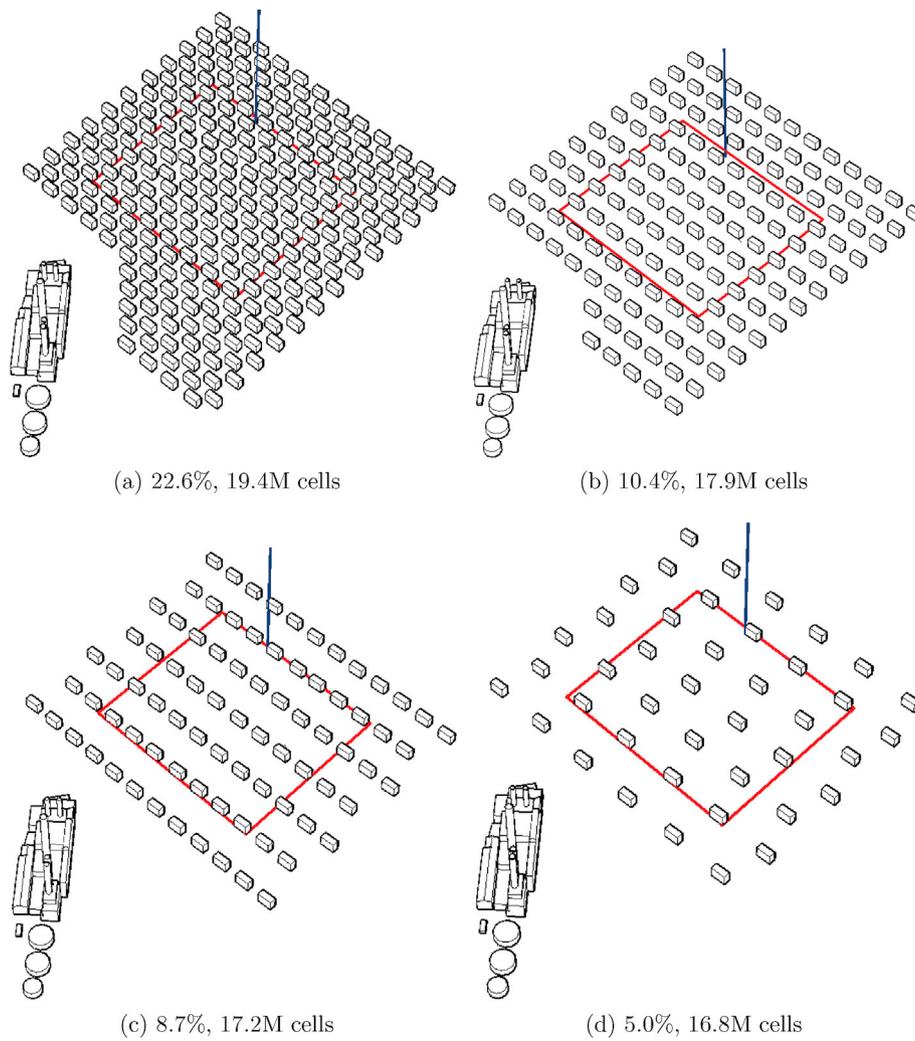
Fig. 8. Geometry of the general patterns with different build densities. The buildings height is 20 m in all the cases. The red square corresponds to the area where the built density is computed, and the blue line corresponds to the axis used for the CO_2 profile comparison. (For interpretation of the references to colour in this figure legend, the reader is referred to the Web version of this article.)
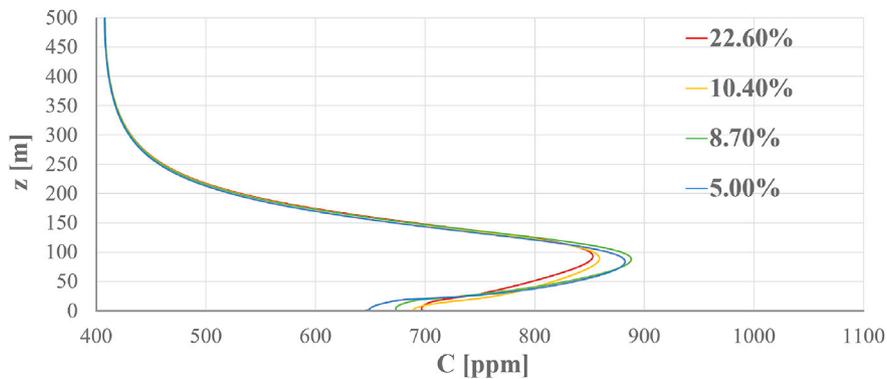
Fig. 9. Vertical profile of CO_2 concentration for different built densities (% of built area), buildings of 20 m height.

observed at the ground level (i.e. below 20 m) due to local effects. Above the buildings, the highest difference occurs for the peak values. Such difference does not show a clear relationship with the density magnitude. The maximum difference observed in this case is 3.7% (7.9% with respect to the background concentration). Therefore, the difference obtained in the CO_2 vertical profile for different built densities is slightly higher than

that obtained for different buildings configuration. However, the simulation results do not reveal a clear dependence of the CO_2 dispersion on the built density because the maximum difference observed between different densities is reasonably low, and a clear relationship is not observed between the density magnitude and the CO_2 profile.
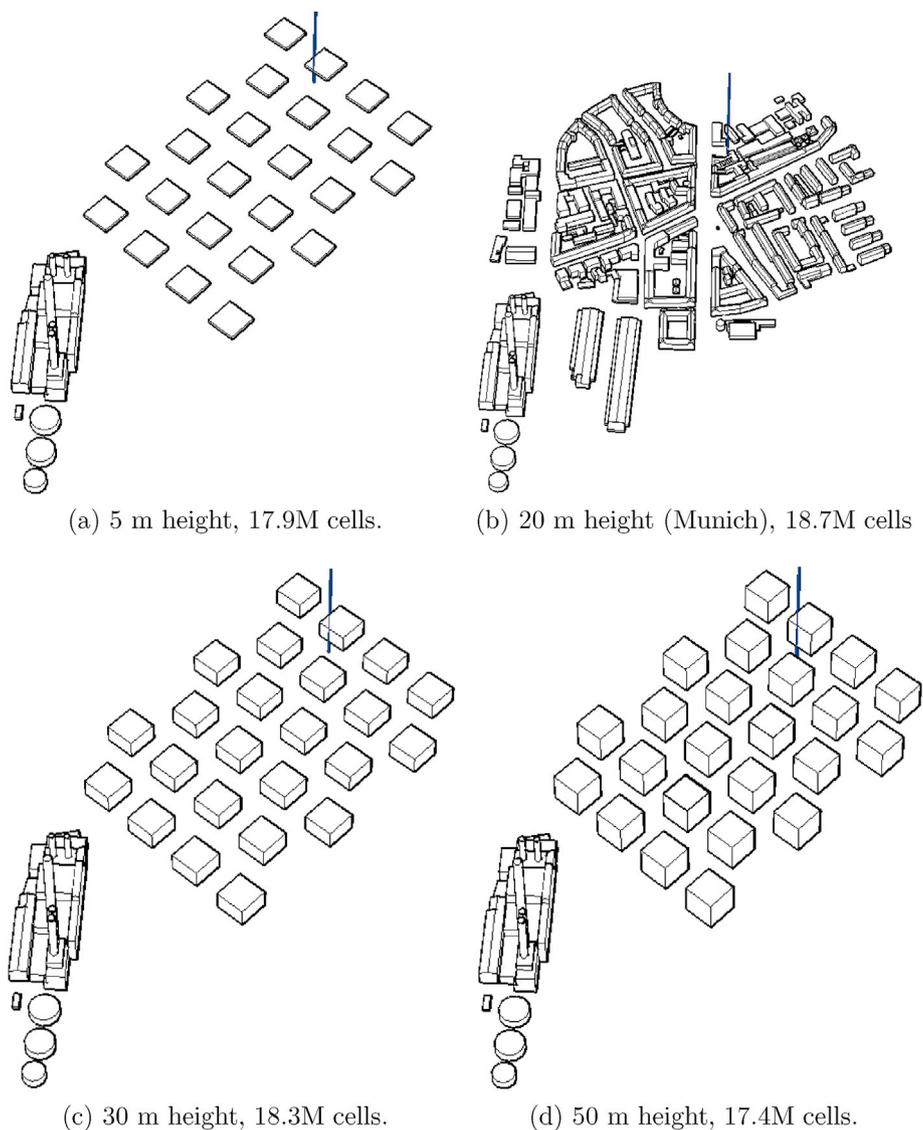
(a) 5 m height, 17.9M cells.   (b) 20 m height (Munich), 18.7M cells

(c) 30 m height, 18.3M cells.   (d) 50 m height, 17.4M cells.

Fig. 10. Geometry used for the study of the in fluence of the buildings height on the CO_2 concentration in the represented axis (blue), including the real geometry of Munich. (For interpretation of the references to colour in this figure legend, the reader is referred to the web version of this article.)
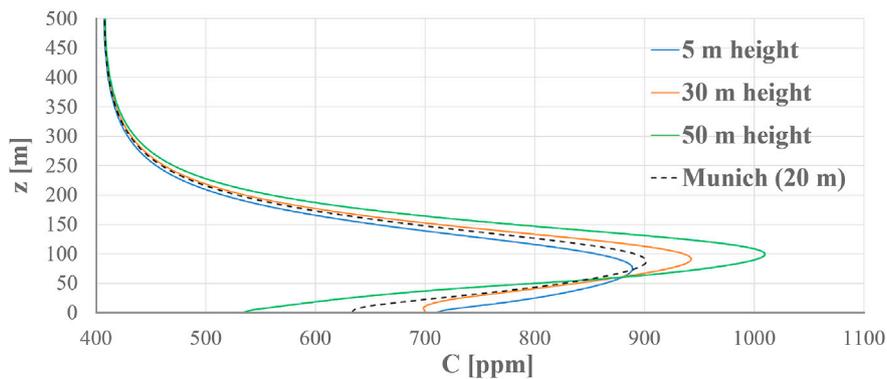

Fig. 11. Vertical profile of CO_2 concentration for different buildings heights.

6. Effect of the buildings height on the gas dispersion

Attending to the evidences in previous sections that suggest that the buildings height has a higher influence on the CO_2 concentration profile, we carry out a comparison of a general pattern with different heights, but with the same buildings distribution and density. As shown in Fig. 10, we compare buildings of 5, 30 and 50 m height, together with the real geometry of Munich which has an averaged height of 20 m. It is observed that the total number of cells used in all the simulations are similar, in order to make fair comparisons. The objective of the geometry
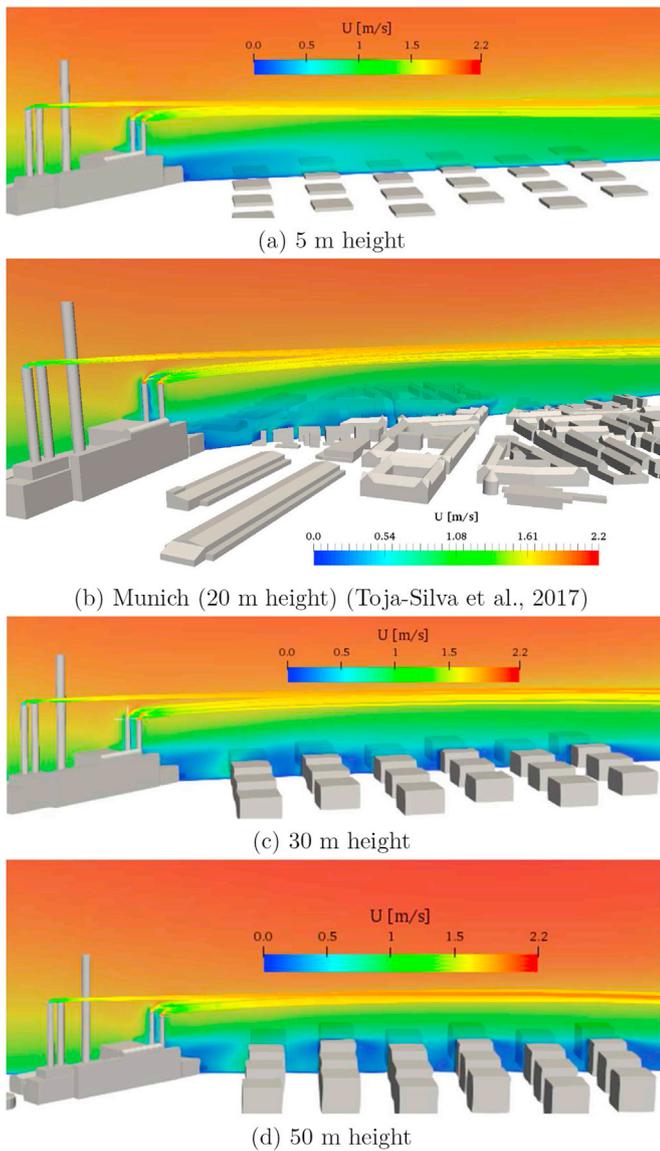
(a) 5 m height

(b) Munich (20 m height) (Toja-Silva et al., 2017)

(c) 30 m height

(d) 50 m height

Fig. 12. Vertical slice of wind velocity for building patterns of different heights, including the streamlines from the chimneys.

generalization is to simplify the preprocessing for the geometry generation, but not necessarily decrease the calculation time. The highest advantage is that the real buildings are not needed, and a simplified city can be designed from simple cartographic information (e.g. using Google Maps (Google,).

The simulation results show that the CO_2 concentration profile has a dependence on the buildings height. As shown in Fig. 11, the peak value of CO_2 concentration increases with the buildings height. The results obtained for 50 m height buildings show a thinner but longer plume, whereas the pattern of 5 m height buildings shows a wider and shorter plume. The rest of the cases, i.e. 20 m (Munich) and 30 m show intermediate plume shapes. This is because the gas diffusion effect is more important for lower buildings, i.e. the convection is more predominant with higher buildings due to a higher wind speed and lower TKE. It is also observed that the higher the buildings height the higher the plume height. This phenomenon is due to the recirculation of the air flow behind the power plant, due to its big dimensions.

The higher wind speed induces a higher convection effect. As shown in Fig. 12, the higher the buildings height the higher the wind speed above the buildings roofs. It is also observed that the plume velocity is higher (i.e. streamlines in Fig. 12) for higher buildings. The streamlines

also show that the plume is higher for higher buildings, i.e. the reason why the peak values in the CO_2 profile are at a higher height for higher buildings. This phenomenon is due to the big wake of the power plant due to its big dimensions, i.e. the air flow falls down behind the power plant. This effect, called downwash effect, occurs without buildings or with low rise buildings, as shown in Fig. 13a. Fig. 13b shows the flow behavior when there are higher buildings, where the air flow climbs up due to the presence of the buildings. This downwash effect is the most important reason why we neglect the effect of the temperature in these simulations.

The gas diffusion effect is more important with lower buildings because the TKE reaches higher values. Fig. 14 shows lower values of TKE above the buildings (i.e. less red color above the buildings for the case of 50 m buildings in Fig. 14d) and at the ground level (i.e. more blue color between the buildings for higher heights) for the high-rise buildings. The same (high) values of TKE are observed around the chimneys in all the cases.

Fig. 15 shows horizontal and vertical slices of CO_2 concentration for the urban patterns of different heights, including the real geometry of Munich. In agreement with the comments above, it is observed a higher gas diffusion effect for the lower buildings, i.e. the plume tends to fall down to the ground level at the last array of buildings in Fig. 15a. On the contrary, the core of the plume does not penetrate between the higher buildings due to a lower diffusion effect (see Fig. 15d).

Fig. 16 shows isosurfaces of the CO_2 concentration. It is observed an enhancement of the street canyon effect (i.e. strong convection inside street canyons due to high wind speed) reported in Toja-Silva et al. (2017) (both up- and down-stream) for the higher buildings. It is clearly observed in Fig. 16c and d (left) how the CO_2 concentration is lower at the ground level when the wind comes from outside of the plume, and vice versa. This street canyon effect (i.e. speed-up in certain streets) causes the unexpected non-homogeneous distribution of CO_2 at the ground level, observed in the horizontal concentration maps in Figs. 7 and 15c (up) and 15d (up).

7. Dispersion coefficient in the Gaussian plume model for different buildings heights

From the simulation results we derive that the buildings height is the most relevant characteristic of an urban environment when replaced by a general pattern. We use these results to improve the vertical dispersion coefficient of the Gaussian plume model, for being used in urban environments of different buildings heights.

The Gaussian plume model (Seinfeld and Pandis, 2006; Reynolds, 1992) consists in a relatively simple expression for computing the mean concentration of a trace gas C (mass per unit volume) under near idealized conditions,

$$C = \frac{Q}{2\pi\sigma_y\sigma_z U}\exp\left(-\frac{y^2}{2\sigma_y^2}\right)\left[\exp\left(-\frac{(z-H)^2}{2\sigma_z^2}\right) + \exp\left(-\frac{(z+H)^2}{2\sigma_z^2}\right)\right],$$

(7)

where x, y and z are the spatial coordinates, Q is the mass flow rate of gas released, H is the emission source height (chimney height), U is the free-stream wind speed (at chimney height), and $\sigma_y(x)$ and $\sigma_z(x)$ are standard deviation in cross-wind and vertical directions, i.e. horizontal and vertical dispersion coefficients respectively. For a neutrally stratified atmosphere (condition assumed in the simulations), the dispersion parameters are defined as (Briggs, 1973)

$$\sigma_y(x) = 0.08x(1 + 0.0001x)^{-\frac{1}{2}}$$

(8)

and

$$\sigma_z(x) = 0.06x(1 + 0.0015x)^{-\frac{1}{2}}.$$
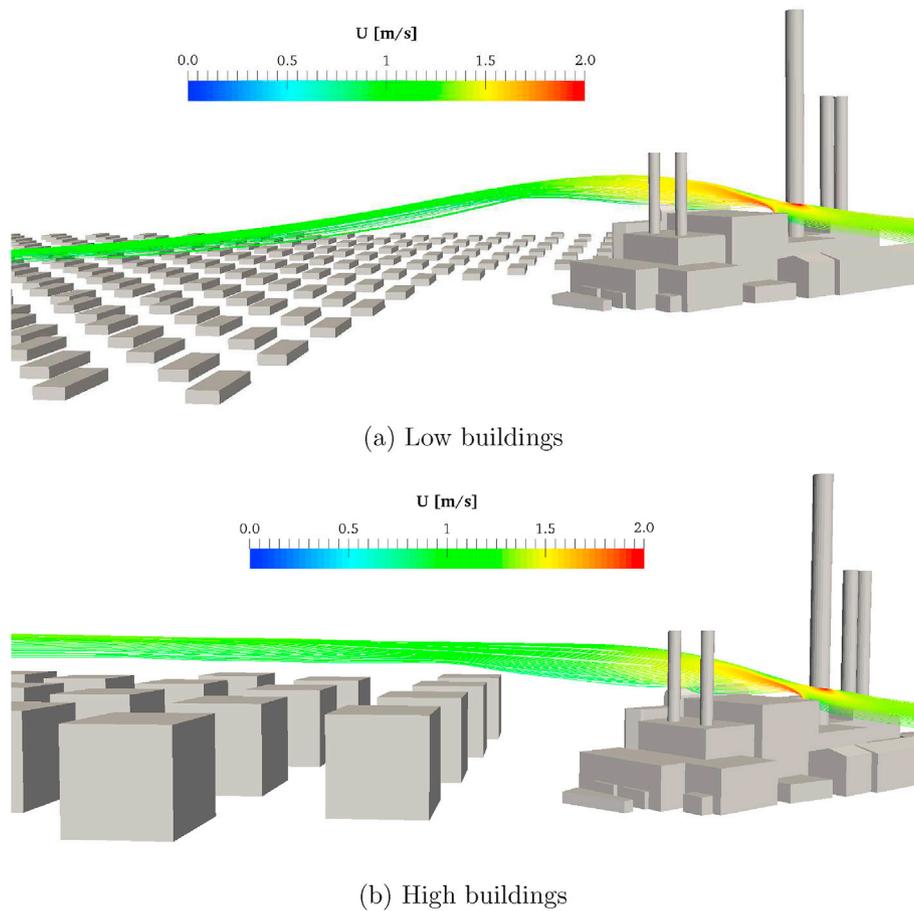
(9)

(a) Low buildings

(b) High buildings

Fig. 13. Streamlines of the air flow behind the power plant, over the buildings.

Briggs (1973) also suggests a specific vertical dispersion parameter for an urban environment,

$$\sigma_z(x) = 0.14x(1 + 0.0003x)^{-\frac{1}{2}}. \tag{10}$$

These dispersion coefficients are recommended by the ALOHA Review Committee (Reynolds, 1992). They are not applicable to every actual ambient situation (United States Environmental Protection Agency, 1980), and they have to be empirically determined from actual atmospheric diffusion experiments or simulations under conditions similar to those of the application (Seinfeld and Pandis, 2006). According to that, Toja-Silva et al. (2017) propose the following expression for the vertical dispersion coefficient yielding a better agreement with the results of numerical simulations using the real geometry of Sending (Munich):

$$\sigma_z(x) = 0.11x(1 + 0.0003x)^{-\frac{1}{2}}. \tag{11}$$

Since we observed in the present investigation that the plume shape (i.e. the dispersion effect) is dependent on the buildings height, we propose a general expression as a function of the buildings height (h) in order to improve Eq. (11):

$$\sigma_z(x, h) = f(h)x(1 + 0.0003x)^{-\frac{1}{2}}, \tag{12}$$

The expression for $f(h)$ used in Eq. (12) is obtained from the optimal value found for the vertical dispersion comparing the Gaussian plume model with CFD simulations of different buildings heights, at a distance of around 500 m downstream of the power plant. Although we studied the simulation results in the whole domain during our investigation, there are several reasons to use this vertical axis for presenting the

quantitative results and extracting the conclusions, i.e.: (*i*) as can be observed in Fig. 15, the plume has a very similar shape within the first 100 m in all the cases and, after that, it changes and shows the effect of the surrounding buildings of different heights; (*ii*) as shown in Fig. 13a, the flow becomes stable over the buildings after more than 200 m downstream, especially for the lower buildings; (*iii*) distances above hundreds of meters are always considered when using the Gaussian plume model (Reynolds, 1992; Briggs, 1973); (*iv*) we can compare the results with those presented in Toja-Silva et al. (2017), where a comparison with experimental measurements is presented.

Fig. 17a shows the vertical profiles of CO_2 obtained in CFD simulations for different buildings heights, and the same vertical profile computed with the Gaussian plume model using the dispersion coefficient that leads to the maximum agreement. It is observed that the height of the plume is always the same using the Gaussian plume model, this is expected because the Gaussian plume model is not able to predict the air flow. The highest difference regarding the plume height is observed for the lowest buildings, because the plume goes down due to the flow recirculation behind the power plant, as explained above.

As shown in Fig. 17b, the optimum value empirically obtained for $f(h)$ has a linear relationship with the buildings heights. Such linear regression yields

$$f(h) = 0.1208 - 0.0006h, \tag{13}$$

and therefore,

$$\sigma_z(x, h) = (0.1208 - 0.0006h)x(1 + 0.0003x)^{-\frac{1}{2}}. \tag{14}$$

Note that only one site (around 500 m downstream) is analyzed in the present short communication. Therefore, Eq. (14) can be verified or
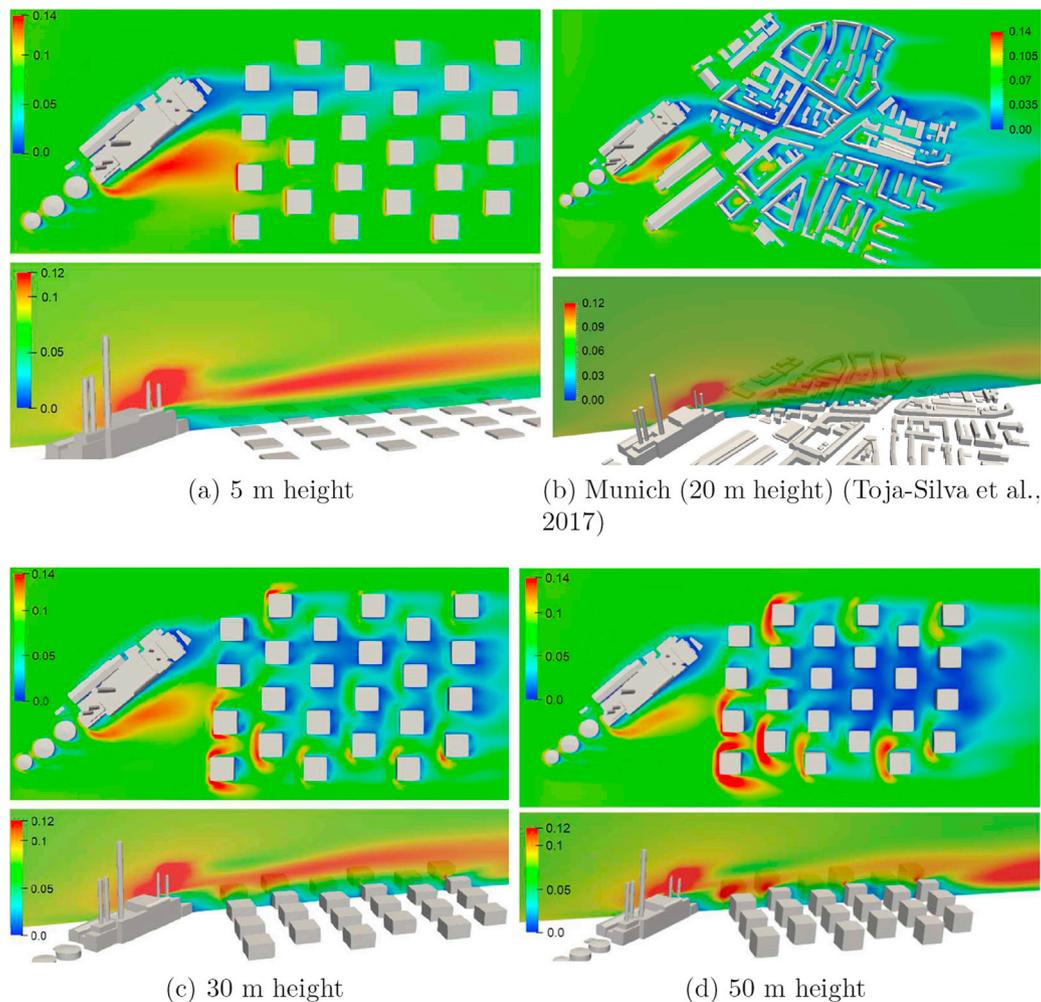
(a) 5 m height

(b) Munich (20 m height) (Toja-Silva et al., 2017)

(c) 30 m height

(d) 50 m height

Fig. 14. Horizontal (at $z = 4\,\mathrm{m}$) and vertical slices of turbulence kinetic energy (k [$\mathrm{m^2/s^2}$]) for building patterns of different heights.

improved (if possible) in further complementary investigations by analyzing different sites and case studies.

8. Verification of the results for an heterogeneous case study

As a verification of the results presented above, we compare the CFD simulation results obtained for Munich with simulation results obtained for an heterogeneous urban environment, i.e. with heterogeneous density and heterogeneous buildings heights (see Fig. 18). Fig. 19 shows the comparison of the CO_2 vertical profiles obtained with these simulations, and with the Gaussian plume model using the vertical dispersion parameter for 20 m. It is observed a reasonably good agreement among the three vertical profiles. As expected, the highest differences take place at the ground level, i.e. between buildings due to local effects explained above. The vertical axis used for the comparison is near higher buildings in the heterogeneous pattern. Additionally, there is a significant difference on the built density, being 19.5% for the heterogeneous pattern and 35.2% for Munich. It is demonstrated thus the independence of the CO_2 vertical profile on the built density. Therefore, we can state that the CO_2 vertical profile is mostly dependent on the averaged building height, regardless of both built density and buildings configuration that cause lower impact on the results.

9. Conclusions

This article is a contribution to the geometry generalization for CFD simulations of gas dispersion in urban areas, with special interest when

dealing with scale ranges between the standard meso- and micro-scales. The CO_2 emission from a natural gas-fueled thermal power plant was simulated using different generic urban patterns, analyzing the influence of buildings distribution, built density and buildings height.

The results from the simulations showed that differences on the urban plant configuration (i.e. buildings distribution and built density) do not have a significant influence on the vertical profile of CO_2 concentration above the city. A marginal difference was observed for different buildings distribution, and a maximum difference of 3.7% for the concentration peak (7.9% with respect to the background concentration) was found for urban patterns with different built density. Of course, higher differences were observed at the ground level (below buildings heights) because the presence (or absence) of a building close to the study site strongly affects locally the values of velocity, TKE and gas concentration.

The average height of the buildings showed a clear influence on the vertical profile of the gas concentration, and such profiles showed a tendency as a function of buildings height. The higher the buildings height, the higher the gas concentration peak above the buildings, and the lower the concentration at the ground level (below buildings height). This is because high buildings induce a high wind speed above the roofs, and turbulent kinetic energy decreases. Therefore, the convective phenomenon enhances and the turbulent diffusion decreases. Additionally, the plume reaches a higher height when the buildings are high. On the opposite, with low buildings, the recirculation of the flow takes place behind the power plant due to its great dimensions and, therefore, the plume descends (downwash effect).

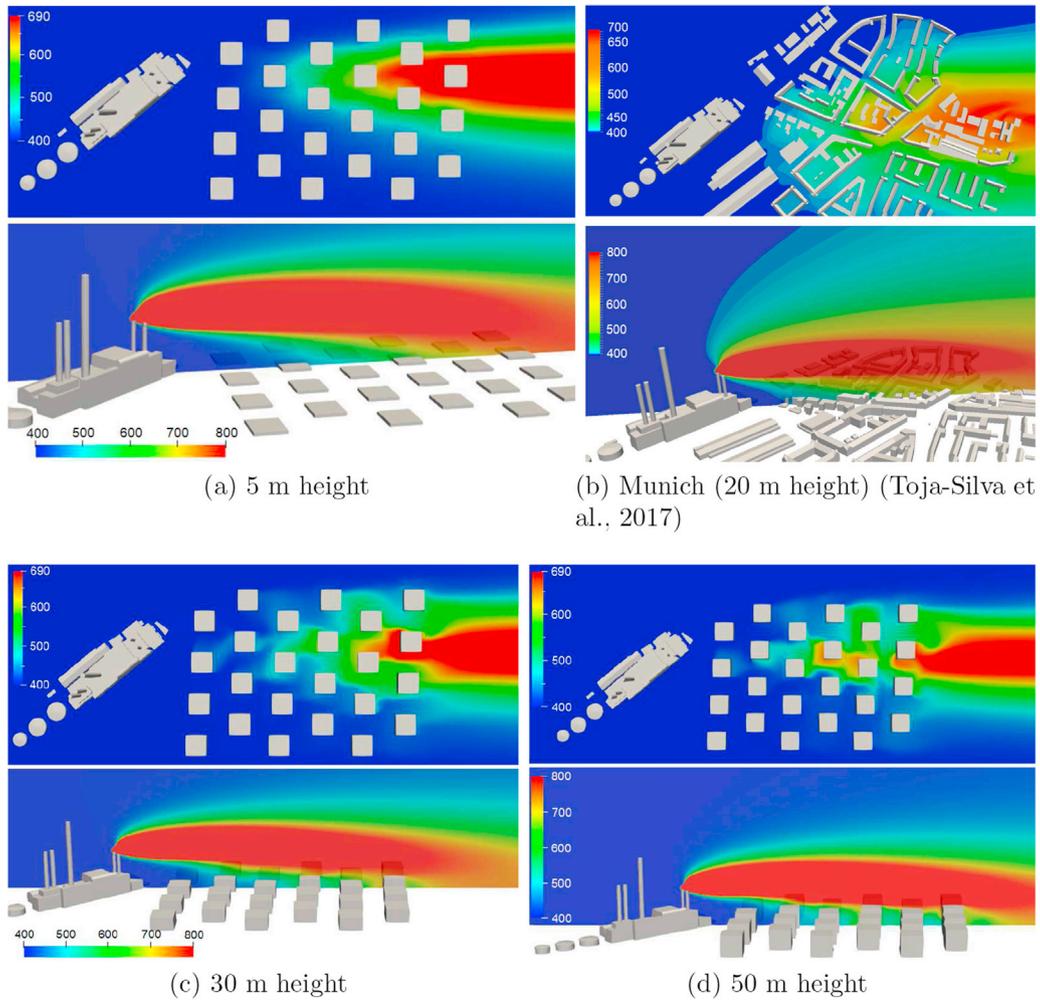The results obtained for the city of Munich (average height near 20 m)

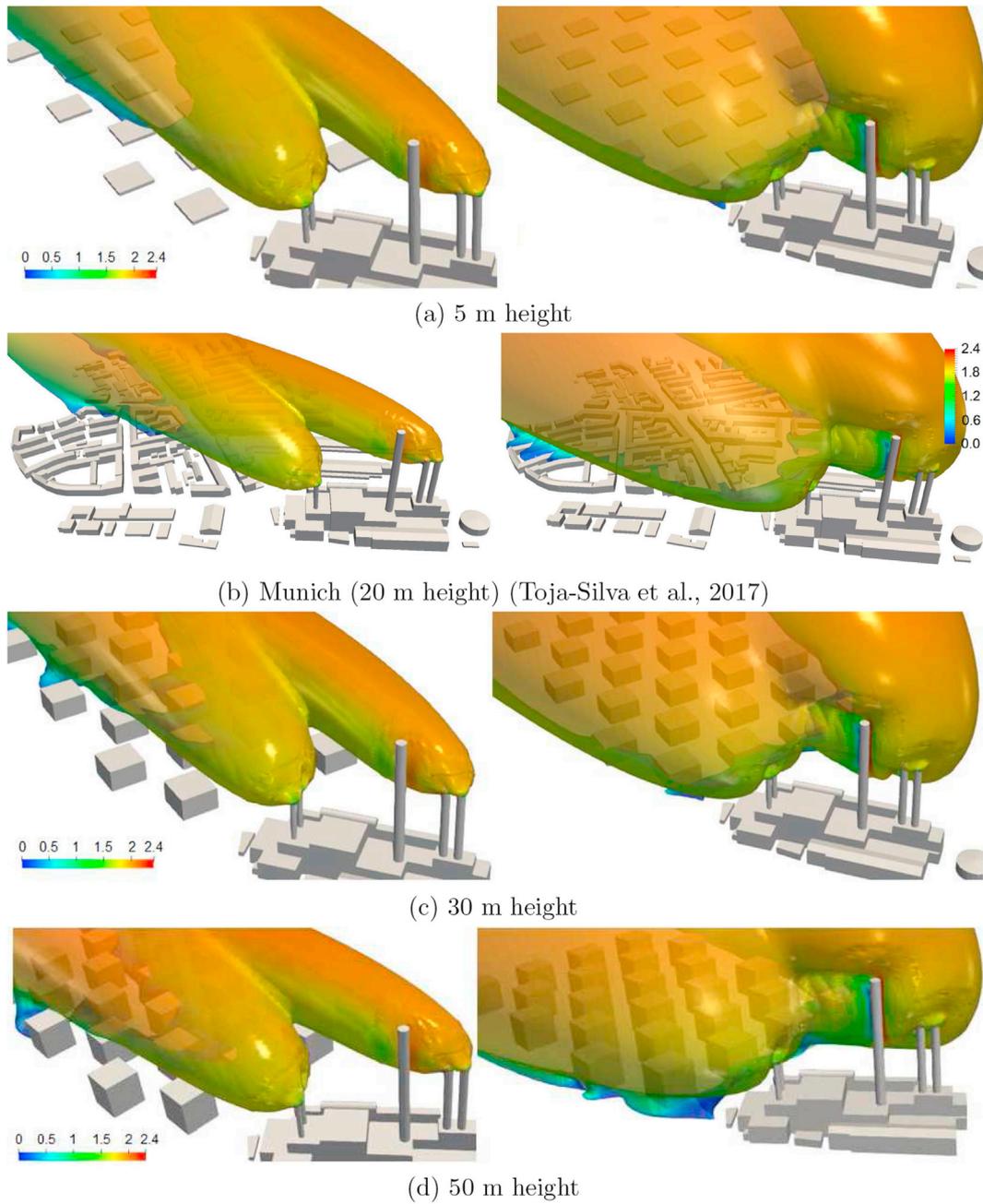(a) 5 m height

(b) Munich (20 m height) (Toja-Silva et al., 2017)

(c) 30 m height

(d) 50 m height

Fig. 15. Horizontal (at $z = 4\,\mathrm{m}$) and vertical slices of CO_2 concentration (C [ppm]) for building patterns of different heights.

(a) 5 m height

(b) Munich (20 m height) (Toja-Silva et al., 2017)

(c) 30 m height

(d) 50 m height

Fig. 16. Isosurfaces of 500 ppm (left) and 403 ppm (right) of CO_2 concentration. Colorbar is wind speed (U [m/s]).

(a) Optimal dispersion coefficient for different buildings heights

$$f(h) = 0.1208 - 0.0006\,h$$
$$R^2 = 0.9934$$
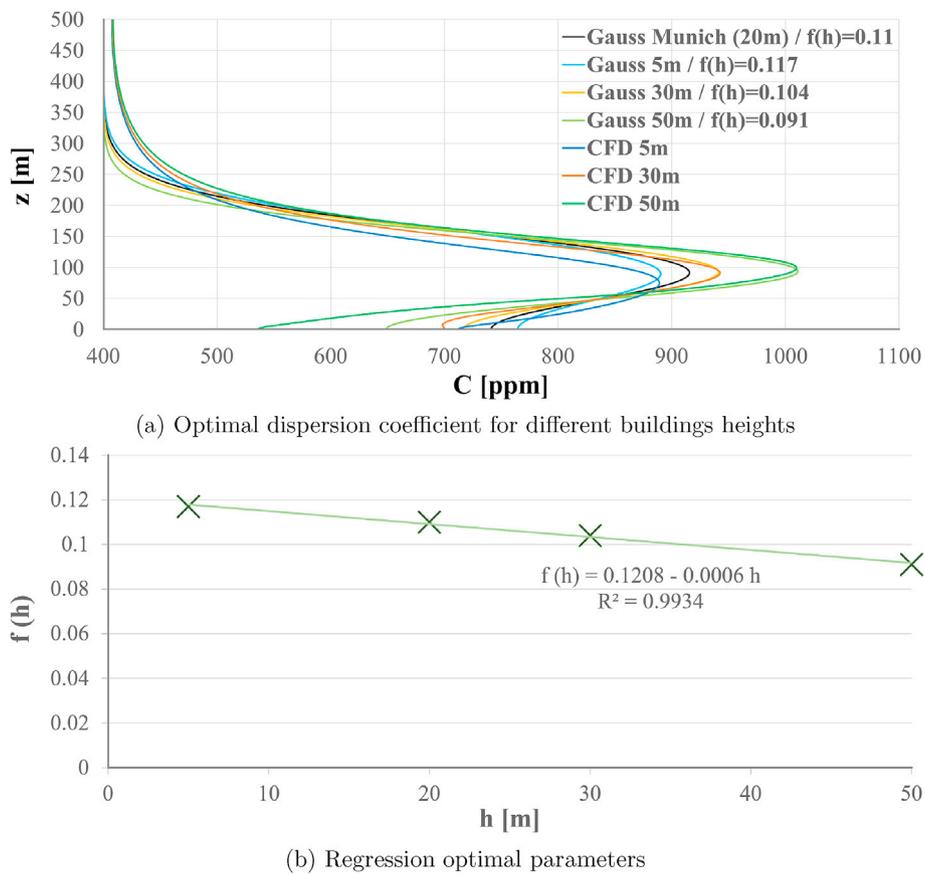
(b) Regression optimal parameters

Fig. 17. Optimal dispersion coefficient for different buildings heights, and linear regression of the parameters.
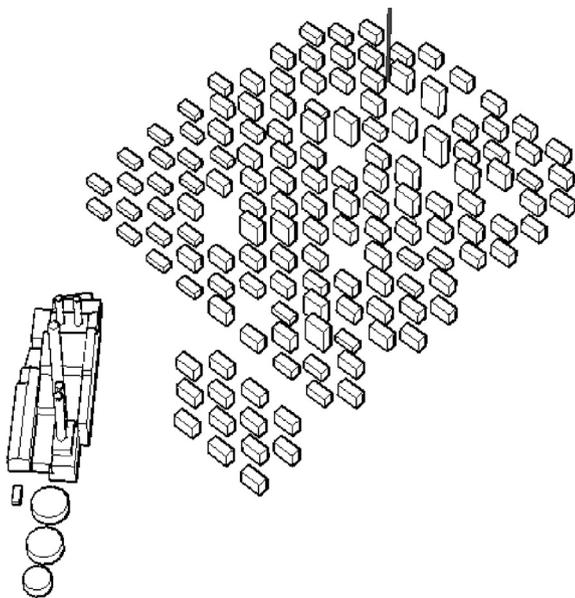

Fig. 18. Geometry of the heterogeneous city, with an averaged height of 20 m.

were compared with those obtained for a pattern composed of buildings with different height (having an average height close to 20 m). A good agreement was observed for the vertical profiles of gas concentration. The most substantial difference takes place below the buildings height due to local phenomena (i.e. street canyon effect).

Regarding the geometry generalization, the final conclusion is that a real city can be replaced by a general pattern with the same averaged height. The objective of the geometry generalization is to simplify the preprocessing for geometry and high-quality mesh generation. The highest advantage is that the real buildings are not needed, and a simplified city can be designed from simple cartographic information. The geometry simplification proposed here aims at two type of problems: when the objective is to analyze the gas dispersion around target buildings immersed in a big urban area, and when the objective is studying the effect of a whole urban area on the gas dispersion, i.e. observed from outside the buildings ensemble, e.g. for determining total city emissions combined with column measurements.

The vertical profiles of gas concentration for different buildings height were also compared with the Gaussian plume model. A new equation for computing the vertical dispersion parameter was empirically derived. Such equation yields the most adequate σ_z for a urban area as a function of its averaged building height. The validity of the empirical equation proposed for the vertical dispersion parameter was demonstrated at around 500 m downstream. The universality of this equation can be verified in further investigations by studying different distances from the source, i.e. different orders of magnitude (e.g. few km).

As future research recommendations, the analysis of other cases (both real cities and generic patterns), and different geometries for the source (power plant) may also be interesting. Additionally, the study of different emission rates and wind speed values would demonstrate that these two factors have no influence on the dispersion parameters used in the Gaussian plume model, an assumption made by all the researchers in the literature. The next step is the simulation of a whole city (or a large urban area), including different simultaneous pollution sources and comparison with experimental measurements.
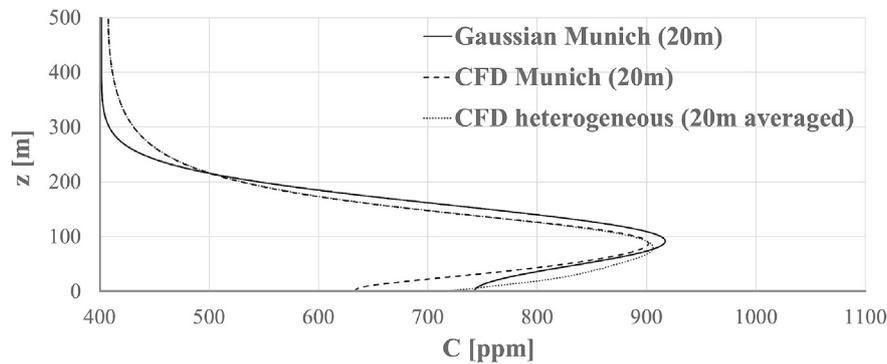
Fig. 19. Vertical profile of CO_2 concentration for different urban environments with an averaged buildings height of 20 m.

References

Architectural Institute Japan (AIJ), 2006. AIJ Benchmarks for Validation of CFD Simulations Applied to Pedestrian Wind Environment Around Buildings. ISBN978-4-8189-5001-6.

Baldasano, J.M., Jiménez-Guerrero, P., Jorba, O., Pérez, C., López, E., Güereca, P., Martín, F., Vivanco, M.G., Palomino, I., Querol, X., Pandolfi, M., Sanz, M.J., Diéguez, J.J., 2008. Caliope: an operational air quality forecasting system for the Iberian Peninsula, Balearic Islands and Canary Islands - first annual evaluation and ongoing developments. Adv. Sci. Res. 2, 89–98.

Beck, V., Koch, T., Kretschmer, R., Marshall, J., Ahmadov, R., Gerbig, C., Pillai, D., Heimann, M., 2011. The WRF Greenhouse Gas Model (WRF-ghg). Technical Report No. 25. Max Planck Institute for Biogeochemistry, Jena (Germany).

Beirle, S., Boersma, K.F., Platt, U., Lawrence, M.G., Wagner, T., 2011. Megacity emissions and lifetimes of nitrogen oxides probed from space. Science 333, 1737–1739.

Bellander, T., Berglind, N., Gustavsson, P., Jonson, T., Nyberg, F., Pershagen, G., Järup, L., 2001. Using geographic information systems to assess individual historical exposure to air pollution from traffic and house heating in Stockholm. Environ. Health Perspect. 109, 633–639.

Blocken, B., Roels, S., Carmeliet, J., 2004. Modification of pedestrian wind comfort in the Silvertop Tower passages by an automatic control system. J. Wind Eng. Ind. Aerod. 92, 849–873.

Blocken, B., Stathopoulos, T., Carmeliet, J., 2007. CFD simulation of the atmospheric boundary layer: wall function problems. Atmos. Environ. 41, 238–252.

Briggs, G.A., 1973. Diffusion Estimation for Small Emissions. ATDL Contribution File 79. Atmospheric Turbulence and Diffusion Laboratory.

Carleton, T.A., Hsiang, S.M., 2016. Social and economic impacts of climate. Science 353. https://doi.org/10.1126/science.aad9837.

Chavez, M., Hajra, B., Stathopoulos, T., Bahloul, A., 2012. Assessment of near-field pollutant dispersion: effect of upstream buildings. J. Wind Eng. Ind. Aerod. 104–106, 509–515.

Chen, J., Viatte, C., Hedelius, J.K., Jones, T., Franklin, J.E., Parker, H., Gottlieb, E.W., Wennberg, P.O., Dubey, M.K., Wofsy, S.C., 2016. Differential column measurements using compact solar-tracking spectrometers. Atmos. Chem. Phys. 16, 8479–8498.

Chen, J., Nguyen, H., Toja-Silva, F., Heinle, L., Hase, F., Butz, A., 2017. Power plant emission monitoring in Munich using differential column measurements. Geophys. Res. Abstr. 19. EGU2017–16423.

Cheng, Y., Lien, F.S., Yee, E., Sinclair, R., 2003. A comparison of Large Eddy Simulations with a standard $k-\varepsilon$ Reynolds-Averaged Navier-Stokes model for the prediction of a fully developed turbulent flow over a matrix of cubes. J. Wind Eng. Ind. Aerod. 91, 1301–1328.

Cimorelli, A.J., Perry, S.G., Venkatram, A., Weil, J.C., Paine, R.J., Wilson, R.B., Lee, R.F., Peters, W.D., Brode, R.W., 2005. AERMOD : a dispersion model for industrial source applications. Part I: general model formulation and boundary layer characterization. J. Appl. Meteorol. 44, 682–693.

Clark, P.U., Shakun, J.D., Marcott, S.A., Mix, A.C., Eby, M., Kulp, S., Levermann, A., Milne, G.A., Pfister, P.L., Santer, B.D., Schrag, D.P., Solomon, S., Stocker, T.F., Strauss, B.H., Weaver, A.J., Winkelmann, R., Archer, D., Bard, E., Goldner, A.,

Lambeck, K., Pierrehumbert, R.T., Plattner, G.-K., 2016. Consequences of twenty-first-century policy for multi-millennial climate and sea-level change. Nat. Clim. Change 6, 360–369.

Cosemans, J., Kretzschmar, J., Maes, G., 1992. The Belgian immission frequency distribution model IFDM. May 6-8. In: Proceedings of the DCAR Workshop on Objectives for the Next Generation of Practical Short Range Atmospheric Dispersion Models. Risø, Roskilde (Denmark).

Durbin, P.A., 1996. On the $k-\varepsilon$ stagnation point anomaly. Int. J. Heat Fluid Flow 17, 89–90.

Feng, S., Lauvaux, T., Newman, S., Rao, P., Ahmadov, R., Deng, A., Díaz-Isaac, L.I., Duren, R.M., Fischer, M.L., Gerbig, C., Gurney, K.R., Huang, J., Jeong, S., Li, Z., Miller, C.E., ÓKeeffe, D., Patarasuk, R., Sander, S.P., Song, Y., Wong, K.W., Yung, Y.L., 2016. Los Angeles megacity: a high-resolution land-atmosphere modelling system for urban CO_2 emissions. Atmos. Chem. Phys. 16, 9019–9045.

Franke, J., Hellsten, A., Schlünzen, H., Carissimo, B., 2007. Best Practice Guideline for the CFD Simulation of Flows in the Urban Environment. COST Action 732. COST Office, Brussels.

Web: Google. https://www.google.de/maps/@48.0980986,11.5528472, 1678a,20y,41.1t/data=!3m1!1e3 (accessed on 1 March 2017).

Gromke, C., Blocken, B., 2015. Influence of avenue-trees on air quality at the urban neighborhood scale. Part I: quality assurance studies and turbulent Schmidt number analysis for RANS CFD simulations. Environ. Pollut. 196, 214–223.

Z.L. Gu, Y.W. Zhang, Y. Cheng, S.C. Lee, Effect of uneven building layout on air flow and pollutant dispersion in non-uniform street canyons. Build. Environ. 46 (12) 2657–2665.

Guevara, M., Tena, C., Soret, A., Serradell, K., Guzmán, D., Retama, A., Camacho, P., Jaimes-Palomera, M., Mediavilla, A., 2017. An emission processing system for air quality modelling in the Mexico City metropolitan area: evaluation and comparison of the MOBILE6.2-Mexico and MOVES-Mexico traffic emissions. Sci. Total Environ. 584–585, 882–900.

Hajra, B., Stathopoulos, T., Bahloul, A., 2011. The effect of upstream buildings on near-field pollutant dispersion in the built environment. Atmos. Environ. 45, 4930–4940.

Hang, J., Li, Y., Sandberg, M., Buccolieri, R., Di Sabatino, S., 2012. The influence of building height variability on pollutant dispersion and pedestrian ventilation in idealized high-rise urban areas. Build. Environ. 56, 346–360.

Hanna, S.R., Brown, M.J., Camelli, F.E., Chan, S.T., Coirier, W.J., Hansen, O.R., Huber, A.H., Kim, S., Reynolds, R.M., 2006. Detailed simulations of atmospheric flow and dispersion in downtown Manhattan. An application of five computational fluid dynamics models. Bull. Am. Meteorol. Soc. 87, 1713–1726.

Jeanjean, A.P.R., Hinchliffe, G., McMullan, W.A., Monks, P.S., Leigh, R.J., 2015. A CFD study on the effectiveness of trees to disperse road traffic emissions at a city scale. Atmos. Environ. 120, 1–14.

Jerrett, M., Arain, A., Kanaroglou, P., Beckerman, B., Potoglou, D., Sahsuvaroglu, T., Morrison, J., Giovis, C., 2005. A review and evaluation of intraurban air pollution exposure models. J. Expo. Anal. Environ. Epidemiol. 15, 185–204.

Kiesewetter, G., Borken-Kleefeld, J., Schöpp, W., Heyes, C., Thunis, P., Bessagnet, B., Terrenoire, E., Fagerli, H., Nyiri, A., Amann, M., 2015. Modelling street level PM_{10} concentrations across Europe: source apportionment and possible futures. Atmos. Chem. Phys. 15, 1539–1553.

Lateb, M., Meroney, R.N., Yataghene, M., Fellouah, H., Saleh, F., Boufade, M.C., 2016. On the use of numerical modelling for near-field pollutant dispersion in urban environments - a review. Environ. Pollut. 208, 271–283.

Lelieveld, J., Evans, J.S., Fnais, M., Giannadaki, D., Pozzer, A., 2015. The contribution of outdoor air pollution sources to premature mortality on a global scale. Nature 525, 367–371.

Lide, D.R., 2004. CRC Handbook of Chemistry and Physics, 85th Edition. CRC Press.

McKain, K., Down, A., Raciti, S.M., Budney, J., Hutyra, L.R., Floerchinger, C., Herndon, S.C., Nehrkorn, T., Zahniser, M.S., Jackson, R.B., Phillips, N., Wofsy, S.C., 2015. Methane emissions from natural gas infrastructure and use in the urban region of Boston, Massachusetts. Proc. Natl. Acad. Sci. Unit. States Am. 112, 1941–1946.

Meng, T., Hibi, K., 1998. Turbulent measurements of the flow field around a high-rise building. J. Wind Eng. 76, 55–64 in Japanese.

Meroney, R., Ohba, R., Leitl, B., Kondo, H., Grawe, D., Tominaga, Y., 2016. Review of CFD guidelines for dispersion modeling. Fluid 1, 1–15.

Nehrkorn, T., Henderson, J., Leidner, M., Mountain, M., Eluszkiewicz, J., McKain, K., Wofsy, S., 2013. WRF simulations of the urban circulation in the Salt Lake City area for CO$_2$ modeling. Journal of Applied Meteorology and Climatology 52, 323–340.

Nosek, Š., Kukačka, L., Kellnerová, R., Jurčáková, K., Jaňour, Z., 2016. Ventilation processes in a three-dimensional street canyon. Boundary-Layer Meteorol. 159, 259–284.

Nosek, Š., Kukačka, L., Jurčáková, K., Kellnerová, R., Jaňour, Z., 2017. Impact of roof height non-uniformity on pollutant transport between a street canyon and intersections. Environ. Pollut. 227, 125–138.

Nozu, T., Tamura, T., 2012. LES of turbulent wind and gas dispersion in a city. J. Wind Eng. Ind. Aerod. 104–106, 492–499.

Web: OpenFOAM. http://www.openfoam.org (accessed on 17 October 2017).

O'Sullivan, J.P., Archer, R.A., Flay, R.G.J., 2011. Consistent boundary conditions for flows within the atmospheric boundary layer. J. Wind Eng. Ind. Aerod. 99, 65–77.

Parente, A., Gorlé, C., van Beeck, J., Benocci, C., 2011. A comprehensive modelling approach for the neutral atmospheric boundary layer: consistent inflow conditions, wall function and turbulence model. Boundary-Layer Meteorol. 140, 411–428.

Patnaik, G., Boris, J.P., Young, T.R., 2007. Large scale urban contaminant transport simulations with Miles. J. Fluid Eng. 129, 1524–1532.

Reynolds, R.M., 1992. ALOHA 5.0: Theoretical Discussion. Technical Memorandum NOS ORCA-65. National Oceanic and Atmospheric Administration, Seattle, WA.

Richards, P.J., Hoxey, R.P., 1993. Appropriate boundary conditions for computational wind engineering models using the $k-\varepsilon$ turbulence model. J. Wind Eng. Ind. Aerod. 46–47, 145–153.

Richardson, L.F., 1911. The approximate arithmetical solution by finite differences of physical problems involving differential equations with an application to the stresses in a masonry dam. Philosophical Transactions of the Royal Society A 210, 459–470.

Saathoff, P., Stathopoulos, T., Wu, H., 1998. The influence of freestream turbulence on nearfield dilution of exhaust from building vents. J. Wind Eng. Ind. Aerod. 77–78, 741–752.

Seinfeld, J.H., Pandis, S.N., 2006. Atmospheric Chemistry and Physics: from Air Pollution to Climate Change. John Wiley & Sons.

Shen, H.H., Cheng, A.H.D., Wang, K.-H., Teng, M.H., Liu, C.C.K., 2002. Environmental Fluid Mechanics: Theories and Applications. ASCE Publications.

Shen, Z., Cui, G., Zhang, Z., 2017. Turbulent dispersion of pollutants in urban-type canopies under stable stratification conditions. Atmos. Environ. 156, 1–14.

Shishegar, N., 2013. Street design and urban microclimate: analyzing the effects of street geometry and orientation on airflow and solar access in urban canyons. Journal of Clean Energy Technologies 1, 52–56.

Snyder, M.G., Venkatram, A., Heist, D.K., Perry, S.G., Petersen, W.B., Isakov, V., 2013. RLINE: a line source dispersion model for near-surface releases. Atmos. Environ. 77, 748–756.

Takano, Y., Moonen, P., 2013. On the influence of roof shape on flow and dispersion in an urban street canyon. J. Wind Eng. Ind. Aerod. 123, 107–120.

Tang, W., Huber, A., Bell, B., Schwarz, W., 2006. Application of CFD simulations for short-range atmospheric dispersion over open fields and within arrays of buildings. In: AMS 14th Joint Conference on the Applications of Air Pollution Meteorology with the A&WMA, Atlanta, GA (USA).

Toja-Silva, F., Peralta, C., Lopez, O., Navarro, J., Cruz, I., 2015. Roof region dependent wind potential assessment with different RANS turbulence models. J. Wind Eng. Ind. Aerod. 142, 258–271.

Toja-Silva, F., Lopez-Garcia, O., Peralta, C., Navarro, J., Cruz, I., 2016. An empirical-heuristic optimization of the building-roof geometry for urban wind energy exploitation on high-rise buildings. Appl. Energy 164, 769–794.

Toja-Silva, F., Chen, J., Hachinger, S., Hase, F., 2017. CFD simulation of CO$_2$ dispersion from urban thermal power plant: analysis of turbulent Schmidt number and comparison with Gaussian plume model and measurements. J. Wind Eng. Ind. Aerod. 169, 177–193.

Tominaga, Y., Stathopoulos, T., 2007. Turbulent Schmidt numbers for CFD analysis with various types of flowfield. Atmos. Environ. 41, 8091–8099.

Tominaga, Y., Stathopoulos, T., 2010. Numerical simulation of dispersion around an isolated cubic building: model evaluation of RANS and LES. Build. Environ. 45, 2231–2239.

Tominaga, Y., Stathopoulos, T., 2013. CFD simulation of near-field pollutant dispersion in the urban environment: a review of current modeling techniques. Atmos. Environ. 79, 716–730.

Tominaga, Y., Stathopoulos, T., 2016. Ten questions concerning modeling of near-field pollutant dispersion in the built environment. Build. Environ. 105, 390–402.

United States Environmental Protection Agency, 1980. OAQPS Guideline Series: Guidelines on Air Quality Models. Research Triangle Park.

van Hooff, T., Blocken, B., 2010. On the effect of wind direction and urban surroundings on natural ventilation of a large semi-enclosed stadium. Comput. Fluids 39, 1146–1155.

von Schneidemesser, E., Kuik, F., Mar, K.A., Butler, T., 2017. Potential reductions in ambient NO$_2$ concentrations from meeting diesel vehicle emissions standards. Environ. Res. Lett. 12, 114025.

Wingstedt, E.M.M., Osnes, A.N., Åkervik, E., Eriksson, D., Pettersson Reif, B.A., 2017. Large-eddy simulation of dense gas dispersion over a simplified urban area. Atmos. Environ. 152, 605–616.

Yoshie, R., Mochida, A., Tominaga, Y., Kataoka, H., Harimoto, K., Nozu, T., Shirasawa, T., 2007. Cooperative project for CFD prediction of pedestrian wind environment in the Architectural Institute of Japan. J. Wind Eng. Ind. Aerod. 95, 1551–1578.

Yu, H., Thé, J., 2016. Validation and optimization of SST $k-\omega$ turbulence model for pollutant dispersion within a building array. Atmos. Environ. 145, 225–238.

Zhang, Y., Kwok, K.C.S., Liu, X.-P., Niu, J.-L., 2015. Characteristics of air pollutant dispersion around a high-rise building. Environ. Pollut. 204, 280–288.